Ingeniería y Competitividad
Vol 27 (1) 2025 doi: 10.25100/iyc.v27i1.14672

Vol 27 (1)

ISSN
0123-3033
e- 2027-8284

Original Article

Application of machine learning models for asbestos cement detection in multispectral images

Aplicación de modelos de aprendizaje automático en la detección de asbesto cemento en imágenes multiespectrales

Gabriel E. Chanchí-Golondrino[1] Manuel A. Ospina-Alarcón[1] Manuel Saba[1]

[1] Universidad de Cartagena, Facultad de Ingeniería, Cartagena de Indias, Colombia

Abstract

Introduction: the detection of asbestos cement has predominantly been carried out using hyperspectral data. The challenge lies in improving detection efficiency without compromising accuracy, especially in contexts where only multispectral images are available.
Objectives: the main objective of this study is to apply machine learning models for the detection of asbestos cement in multispectral images.
Methodology: the research was conducted using a four-phase adaptation of the CRISP-DM methodology, which included the following steps: Dataset creation: A dataset was compiled and prepared from a reference multispectral image of the city of Cartagena. Evaluation of relevant bands: The most relevant spectral bands for detecting asbestos cement were selected. Model training and evaluation: Four machine learning models were trained and evaluated: kNN, decision trees, support vector machines (SVM), and logistic regression. Deployment of the best model: Finally, the best-performing model was deployed on the reference image to assess its performance in a real-world scenario.
Results: of the four models evaluated, the decision tree model demonstrated the highest efficiency and consistency on both the training and testing sets, achieving a value of 0.93 for both Precision and Recall metrics. In contrast, the logistic regression model performed the worst, with values of 0.829 and 0.875 for Precision and Recall, respectively.
Conclusions: the proposed decision tree model proved to be an effective and consistent tool for detecting asbestos cement in multispectral images, with a good balance between precision and recall. This model provides a viable solution for automatic material detection in contexts where only multispectral images are available and can serve as a reference in both academic and industrial settings for integration into material detection systems.

Keywords: Asbestos detection, machine learning, multispectral imaging, remote sensing.

Resumen

Introducción: La detección de asbesto cemento ha sido predominantemente realizada utilizando datos hiperespectrales. El desafío radica en mejorar la eficiencia de la detección sin comprometer la precisión, especialmente en contextos donde solo están disponibles imágenes multiespectrales.
Objetivos: El objetivo principal de este estudio es aplicar modelos de aprendizaje automático para la detección de asbesto cemento en imágenes multiespectrales.
Metodología: La investigación se llevó a cabo utilizando una adaptación de cuatro fases de la metodología CRISP-DM, que incluyó los siguientes pasos: Creación del dataset: Se recopiló y preparó un conjunto de datos a partir de una imagen multiespectral de referencia de la ciudad de Cartagena. Evaluación de las bandas relevantes: Se seleccionaron las bandas espectrales más relevantes para la detección de asbesto cemento. Entrenamiento y evaluación de modelos: Se entrenaron y evaluaron cuatro modelos de aprendizaje automático: kNN, árboles de decisión, máquinas de soporte vectorial (SVM) y regresión logística. Despliegue del mejor modelo: Finalmente, el modelo con mejor rendimiento fue desplegado sobre la imagen de referencia para evaluar su desempeño en un escenario real.
Resultados: de los cuatro modelos evaluados, el modelo de árboles de decisión demostró la mayor eficiencia y consistencia en los conjuntos de entrenamiento y prueba, logrando un valor de 0.93 tanto en las métricas de Precisión como de Recall. En contraste, el modelo de regresión logística fue el que obtuvo el peor rendimiento, con valores de 0.829 y 0.875 en Precisión y Recall, respectivamente.
Conclusiones: el modelo propuesto de árboles de decisión demostró ser una herramienta efectiva y consistente para la detección de asbesto cemento en imágenes multiespectrales, con un buen balance entre precisión y recall. Este modelo ofrece una solución viable para la detección automática de materiales en contextos donde solo se disponen de imágenes multiespectrales y puede servir como referencia tanto en el ámbito académico como industrial para su integración en sistemas de detección de materiales.

Palabras clave: Detección de asbesto, aprendizaje automático, imágenes multiespectrales, sensado remoto**.**

How to cite?

Chanchi-Golondrino, G.E., Ospina-Alarcón, M.A., Saba, M. Application of machine learning models for asbestos cement detection in multispectral images. Ingeniería y Competitividad, 2025, 27(1)e-21014672

https://doi.org/10.25100/iyc.v27i1.14672

Received: 30/12/24
Reviewed: 10/03/24
Accepted: 14/03/25
Online: 19/03/25

Correspondence

gchanchig@unicartagena.edu.co

Contribution to the literature

Considering Colombian legislation that prohibits the use of asbestos-cement due to its implications for public health, conducting research focused on the automated detection of asbestos-cement becomes relevant, leveraging the advantages provided by remote sensing and computer vision techniques. In this regard, given the large volume of information contained in hyperspectral images and the associated computational resource demands, it is necessary to identify computational methods that enable the detection of asbestos-cement in lower-dimensional scenarios, such as multispectral images.
In this research, a machine learning workflow was deployed on a dataset of spectral signatures of asbestos-cement and other materials, extracted from a multispectral image of the city of Cartagena de Indias. The workflow was implemented using the Orange visual programming tool, allowing the evaluation of four machine learning models (kNN, Decision Trees, Support Vector Machines, and Logistic Regression). The results indicated that the Decision Tree model achieved the best and most consistent performance, with a Precision and Recall score of 0.93. Additionally, it was determined that the most relevant bands for asbestos identification are bands 8 and 5, demonstrating that the presence of the material can be detected using only these two bands from the multispectral image. These findings make a significant contribution to computational efficiency in multispectral image processing, as it is unnecessary to process all eight reflectance bands, thereby enhancing environmental monitoring systems based on remote sensing.

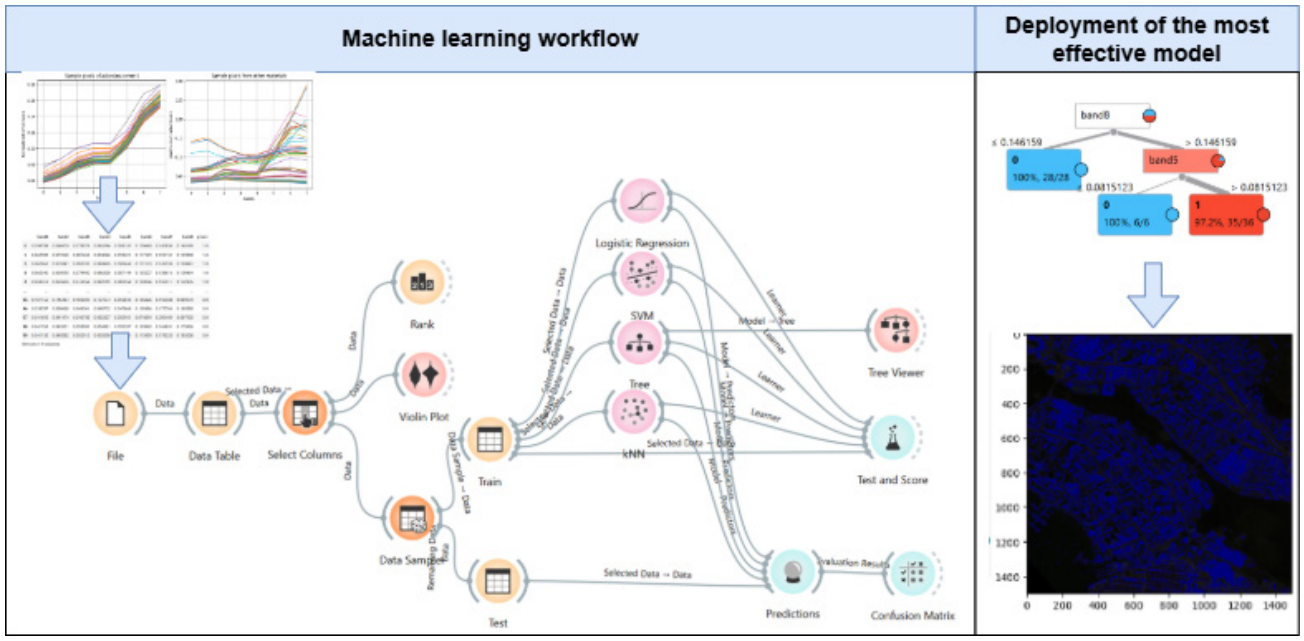

doi: 10.25100/iyc.v27i1.14672

Introduction

Remote sensing, also known as teledetection, refers to the science dedicated to acquiring and processing information about the Earth's surface through the use of sensors mounted on drones, airplanes, and satellites. By analyzing the interaction of electromagnetic energy with surface objects, it is possible to obtain data related to their physical and chemical properties without requiring physical contact (1–3). In the context of multispectral images, leveraging information from various spectra, such as visible and infrared, enables robust and reliable object detection in open environments (4,5). Compared to object detection using RGB images, multispectral imaging has proven to be more accurate across different settings, offering an effective solution under conditions of low illumination and adverse weather, where RGB images often fail (4,6,7).

Multispectral images have been widely applied across various fields for material detection and classification. In agriculture, they have been instrumental in identifying plant species based on their spectral signatures, facilitating the detection of areas prone to pests and assessing crop conditions, such as in coffee plantations, through both conventional and drone-captured images (8–10). Recent advancements in machine learning have further enhanced the applications of multispectral imaging in agricultural monitoring. For instance, high-resolution multispectral images collected via UAVs, combined with Support Vector Machine (SVM) models, have been used to estimate key agronomic variables in flooded rice cultivation. This approach demonstrated strong correlations for predicting leaf area index (LAI), nitrogen content (Narea), and grain yield, achieving a Pearson correlation coefficient of up to 0.89 in training and 0.87 in testing (11).

Similarly, in the environmental context, digital processing of satellite images has been shown to effectively monitor phenomena such as land degradation by analyzing image variations over time (12). The integration of multispectral images with object-based image analysis (OBIA) methods has been successfully employed in classifying mangrove species within wetland ecosystems. A study conducted in Dong Rui Commune, northern Vietnam, used Phantom 4 UAVs to acquire spectral reflectance data for tree species classification, achieving an overall accuracy of 91.11% and a kappa coefficient of 0.87. This method provided a reliable basis for wetland conservation planning and species monitoring, demonstrating the potential of multispectral imaging in ecological research (13).

Moreover, the high spectral resolution of multispectral images has enabled detailed analysis of vegetation conditions, including the detection of specific components such as nutrients and pigments like chlorophyll (14–16). The fusion of multispectral imaging with deep learning techniques has further improved agricultural monitoring, as evidenced by a study on MD2 pineapple crops in Colombia. Using UAV-derived multispectral data, in situ ecological sensor data, and machine learning techniques such as Extreme Gradient Boosting (XGBoost) and Multilayer Perceptron (MLP) regressors, researchers achieved nitrogen content estimation with a determination coefficient (R^2) of up to 86.98%. This study underscores the importance of integrating multispectral imaging with advanced computational models to enhance nutrient diagnostics and optimize agricultural management (17).

doi: 10.25100/iyc.v27i1.14672

Beyond environmental applications, multispectral images have proven effective in food quality control and classification. The combination of reflectance and autofluorescence-based multispectral imaging with machine learning algorithms has been successfully employed to differentiate special and traditional green coffee beans. In this context, SVM models achieved an impressive accuracy of 96% in classifying green coffee, with autofluorescence data playing a crucial role in distinguishing different coffee types based on their chemical compositions (18).

Furthermore, integrating multispectral images with radar data enhances the ability to monitor species distribution and ecosystem structures, which is particularly valuable for biodiversity conservation (19). Multispectral imaging has also demonstrated significant potential in detecting objects under limited visibility conditions, such as those encountered during search and rescue operations when combined with deep learning techniques (20). In geological applications, multispectral images have been utilized for mineral mapping, allowing for the identification of compounds such as kaolinite, illite, alunite, calcite, dolomite, hematite, goethite, and quartz. Additionally, these images facilitate the simultaneous mapping of alteration zones, such as propylitic and argillic zones, which are crucial for mineral exploration and the mining industry (21,22).

Therefore, multispectral imaging, particularly when integrated with machine learning models, has significantly advanced the accuracy and efficiency of classification and detection tasks across various domains. From precision agriculture and wetland conservation to food quality control and mineral exploration, the combination of high-resolution spectral data with computational techniques continues to enhance analytical capabilities, offering new insights and practical solutions in diverse fields.

Regarding the detection of asbestos cement, which is the main focus of this research, it is important to highlight that hyperspectral images have been primarily used for the effective detection and classification of asbestos in cement products. These methods enable the identification of different types of asbestos minerals, such as amosite, crocidolite, and chrysotile, leveraging their unique spectral signatures in the shortwave infrared range (SWIR: 1000–2500 nm) (23). Similarly, hyperspectral images have been employed to assess the deterioration state of asbestos cement roofs, contributing to the mapping and prioritization of the removal of these hazardous materials that pose significant health risks (24,25).

Additionally, convolutional neural networks and other classification techniques have been effectively applied to identify asbestos cement roofs using data derived from hyperspectral images, demonstrating that high spectral resolution is crucial for accurate classification and discrimination of asbestos (26). These prior investigations are particularly relevant for public health, as asbestos is a known carcinogen associated with mesothelioma and cancers of the lung, larynx, and ovary, with even low-level exposure significantly increasing the risk of developing these diseases (27–29).

Considering that hyperspectral images have been widely and effectively used in asbestos detection through remote sensing techniques, it is important to highlight that the high dimensionality of these images necessitates efficient memory usage and the implementation of high-performance architectures based on parallel computing (30–32). Additionally, given that hyperspectral images

doi: 10.25100/iyc.v27i1.14672

contain a large number of bands, some of which may be redundant, dimensionality reduction techniques are required to facilitate their interpretation and classification (33–35).

This high dimensionality can increase processing times, making it essential to employ more efficient algorithms or methods capable of managing complexity without compromising accuracy (32,36). The complexity inherent in hyperspectral image processing is significantly reduced when processing satellite multispectral images, which require lower computational demand and consume less energy (37–39). Therefore, it becomes necessary to evaluate and select the most suitable models for the context of satellite images to enable the efficient detection of asbestos cement without sacrificing accuracy.

This article proposes the application of machine learning models for the detection of asbestos cement in satellite multispectral images as a contribution, aiming to identify the model with the highest classification accuracy for asbestos based on the appropriate characterization of its spectral signature. To achieve this, a dataset was initially constructed, comprising 100 observations of 8 attributes corresponding to the spectral information of 8 bands from 50 pixels of asbestos cement and 50 pixels of other materials. It is worth noting that the dataset observations were sampled from a reference VNIR (Visible and Near-Infrared) multispectral image obtained from the city of Cartagena, Colombia, featuring 8 spectral bands covering both the visible spectrum (425.0 nm to 660.0 nm) and the near-infrared spectrum (725.0 nm to 950.0 nm).

This dataset was used to train and validate four machine learning models utilizing the Orange visual programming tool. Similarly, for deploying the model with the best performance and consistency in both the training and testing sets, the advantages provided by libraries such as Spectral, NumPy, pandas, and Scikit-learn were leveraged to implement and evaluate the model on the complete reference image, which has dimensions of 1500x1500 pixels, each containing eightspectral bands. The Visual Orange tool was selected, considering that it provides a graphical interface that facilitates the visual construction of machine learning workflows, enabling both novices and experts to perform complex analyses, such as image classification and clustering, without the need for programming (40).

The results of this research aim to serve as a reference for academic and industrial applications in the integration of environmental systems for material detection in multispectral images. The remainder of the article is organized as follows: Section 2 describes the methodological approach, Section 3 presents the results, and Section 4 outlines the conclusions and future research directions.

Methodology

For the development of this research, the CRISP-DM methodology was adapted into four phases: P1. Business and Data Understanding, P2. Data Preparation, P3. Modeling and Evaluation, and P4. Model Deployment (see Figure 1). Although Figure 1 presents the methodology in a sequential manner, it is important to note that CRISP-DM is an iterative process. In practice, if the model's performance is not optimal, it may be necessary to revisit previous phases, such as data preparation or feature selection, to refine the results. This cyclical nature ensures continuous

doi: 10.25100/iyc.v27i1.14672

improvement and adaptation throughout the modeling process. This methodology was adapted considering that it is a standard process model widely used for the development of data mining and machine learning projects, with the advantage of being independent of the industrial sector and the type of technology employed, making it applicable to diverse contexts (41–44).

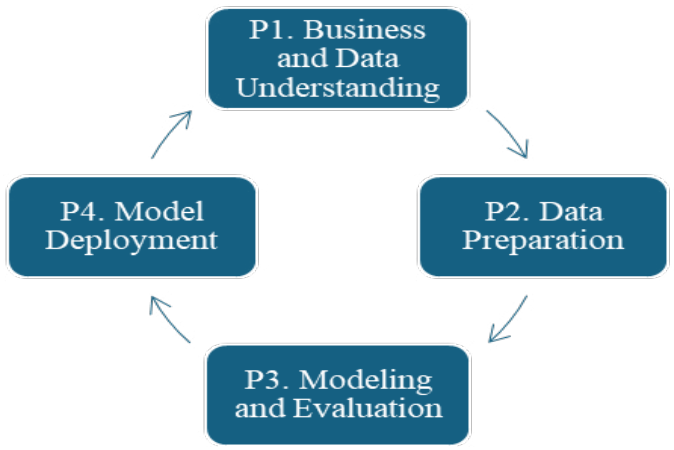

Figure 1. Methodology considered. Source:own elaboration.

In Phase 1 of the methodology, tools for accessing spectral band information from satellite images were initially explored, identifying that the Python libraries Spectral and NumPy enable the processing of spectral band data from such images. Using these selected libraries and based on a pre-processed 8-band VNIR multispectral image of 1500x1500 pixels from the city of Cartagena, which underwent atmospheric correction, data corresponding to 50 pixels of asbestos cement and 50 pixels of other materials were extracted. It is worth mentioning that the sample pixels were selected through visual inspection of an RGB representation of the multispectral image, choosing roofs located in areas where field visits and verification tests had previously been conducted by the professionals involved in the project within which this research is framed. Accordingly, Figure 2 presents the RGB representation of the reference satellite image, where the 50 sampled pixels of asbestos are highlighted in blue, and the 50 pixels of other materials are marked in red.

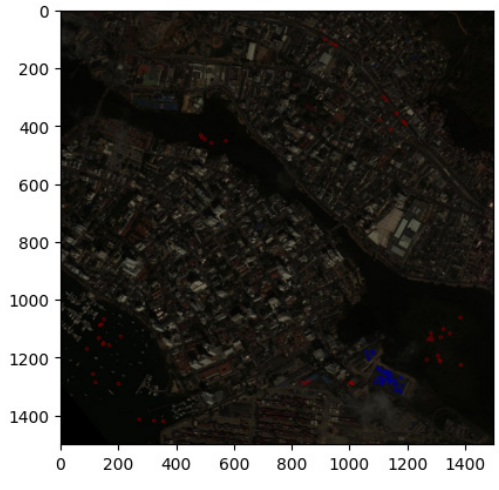

Figure 2. Sample pixels selected from asbestos cement and other materials. Source: own elaboration.

doi: 10.25100/iyc.v27i1.14672

In Phase 2 of the methodology, the data from the 8 bands of the 50 asbestos pixels were normalized and labeled with a value of 1, while the data corresponding to the 8 bands of the 50 pixels of other materials were labeled with a value of 0, using the Pandas and NumPy libraries. The normalization was performed by identifying the maximum and minimum reflectance values to scale the data accordingly. These data were then integrated and organized into a dataframe structure to create the working dataset.

The dataset contains an equal number of instances labeled as asbestos and other materials, indicating a balanced class distribution, which is essential to prevent models from developing biases or inherently favoring one of the two defined labels, thereby ensuring a more equitable and representative training process.

To facilitate further processing, this dataset was exported to an Excel file for subsequent loading into the machine learning workflow of the Orange tool. Accordingly, Figure 3 presents both the 50 spectral signatures of the asbestos pixels and the spectral signatures of the 50 non-asbestos pixels included in the dataset. It is evident that for each material, the spectral signatures report the normalized reflectance values across the 8 spectral bands.

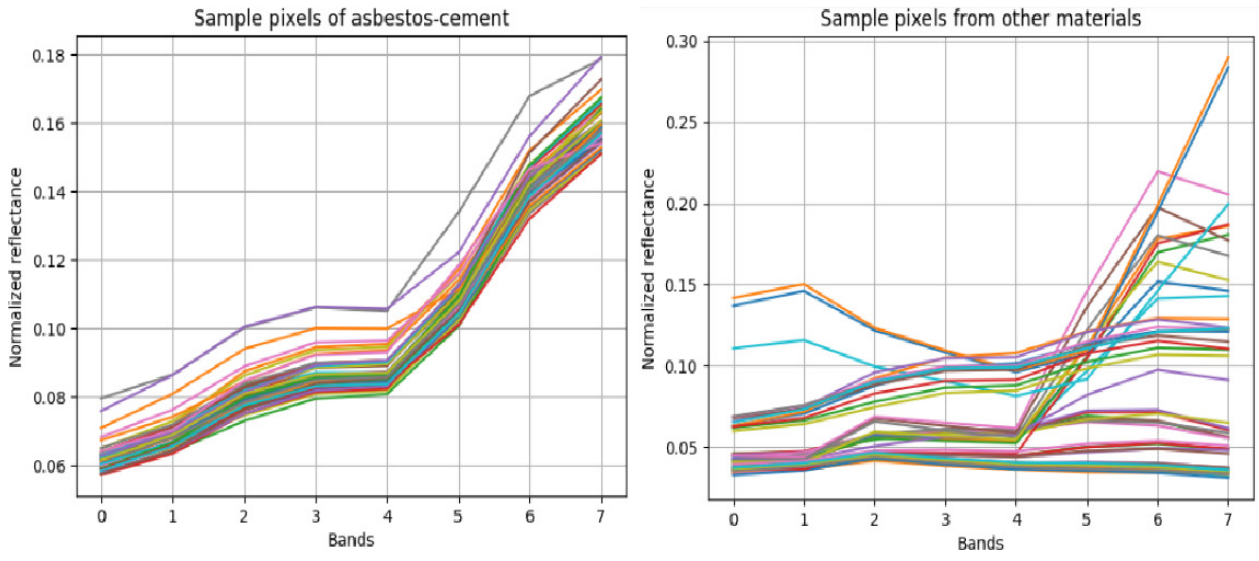

Figure 3. Sample pixels selected from asbestos cement and other materials. Source: own elaboration.

Similarly, Table 1 shows the dataset constructed from the spectral signatures presented in Figure 3, where each spectral signature was labeled with a 1 or a 0, depending on whether it corresponds to asbestos cement or another material. The dataset comprises 100 instances, each containing 9 columns: the first 8 columns represent the reflectance values for the respective spectral bands, and the 9th column contains the label assigned according to the type of material.

doi: 10.25100/iyc.v27i1.14672

Table 1. Sample pixels selected from asbestos cement and other materials

Instance	Band 1	Band 2	Band 3	Band 4	Band 5	Band 6	Band 7	Band 8	Pixel
0	0.05979	0.06693	0.07807	0.08426	0.08514	0.10567	0.14085	0.16016	1
1	0.06298	0.07184	0.08747	0.09453	0.09542	0.11713	0.15215	0.16987	1
2	0.06296	0.07049	0.08320	0.08989	0.09066	0.11107	0.14334	0.15987	1
3	0.06235	0.06959	0.07991	0.08633	0.08715	0.10551	0.13862	0.15846	1
4	0.05951	0.06591	0.07627	0.08221	0.08296	0.10309	0.13552	0.15231	1
...	...	...	...	...	...	...	...	...	...
95	0.13716	0.14646	0.12032	0.10737	0.09584	0.10583	0.19554	0.28928	0
96	0.03956	0.03842	0.04956	0.04873	0.04787	0.10939	0.17577	0.18053	0
97	0.04169	0.04147	0.04678	0.05234	0.05395	0.07482	0.09049	0.08792	0
98	0.04176	0.04333	0.05508	0.05436	0.05339	0.10384	0.16483	0.17557	0
99	0.04113	0.04058	0.05251	0.05329	0.05305	0.11339	0.17822	0.18324	0

100 rows x 9 columns

In Phase 3 of the methodology, the attributes of the dataset were initially analyzed using information gain methods (Gain Ratio and Chi-Square), which are well-known for their effectiveness in identifying the relevance of attributes in relation to the target variable, and violin plots, which enable simultaneous visualization of data distribution and density within each category of the predictor attribute. This facilitated a precise estimation of the attributes with the greatest impact on the predictor attribute, which in this case corresponds to the material type (pixel column).

Within this phase, the data were split into training and testing sets using the Data Sampler component in Orange. Four conventional machine learning models: KNN, support vector machines, logistic regression, and decision tree, were then trained and fine-tuned using the training set. It is worth mentioning that conventional machine learning models were chosen, considering that although deep learning-based models exhibit high effectiveness, they often require complex network structures and large volumes of data, which can be intensive in terms of processing time and computational resources, making them unsuitable for environmental monitoring applications (45). Finally, evaluation components were integrated into the Orange workflow to assess the models on both the training and testing sets, obtaining key evaluation metrics (accuracy, precision, recall, and F1-score), as well as the confusion matrix for the testing set. Based on the results of these metrics, the model with the best consistency and performance across training and testing was selected for application to the complete reference image. It is worth mentioning that the AUC-ROC metric was not considered, as it is more useful and provides significant information in the context of imbalanced datasets (46).

In Phase 4 of the methodology, the model with the best performance and consistency was implemented and applied to the entire multispectral image, leveraging the advantages provided by the Python libraries Spectral, Pandas, Scikit-learn, and NumPy. Additionally, based on the detection performed by the method across the entire image, the percentage of pixels corresponding to asbestos was determined. The resulting percentage is of particular interest to environmental authorities for identifying asbestos roofs in the neighborhoods of Cartagena.

doi: 10.25100/iyc.v27i1.14672

In accordance with the above, the present study aims to address the following questions: What is the performance of machine learning methods for asbestos detection in multispectral images?, What is the efficacy and efficiency of the best-performing model compared to conventional methods?, In which application fields can the proposed approach be extrapolated?

Results

Regarding the results, the dataset from Table 1 was first loaded into the Orange visual programming tool, and the "Rank" module was applied to determine the attributes with the greatest impact on the predictor attribute. This was achieved using the Gain Ratio and Chi-Square methods, with the results presented in Figure 4.

According to the results presented in Figure 4, the Gain Ratio and Chi-Square methods identified that the bands providing the most significant contribution to the predictor attribute (dataset pixel column) are bands 8, 2, and 5, each with an information gain percentage exceeding 20.9%. Band 8 was the most relevant, with a Gain Ratio value of 0.264 and a Chi-Square contribution of 27.307.

It is possible to observe how bands 2 (480 nm, blue), 5 (660 nm, red), and 8 (950 nm, near-infrared) may be key for the detection of asbestos-cement due to their interaction with the spectral composition of the material. Band 2 highlights its reflectance in the visible range, Band 5 captures the absorption of characteristic minerals, and Band 8 enables differentiation through its response in the infrared. These bands, collectively, appear to optimize the identification of asbestos-cement by capturing its distinctive spectral properties across different ranges of the electromagnetic spectrum.

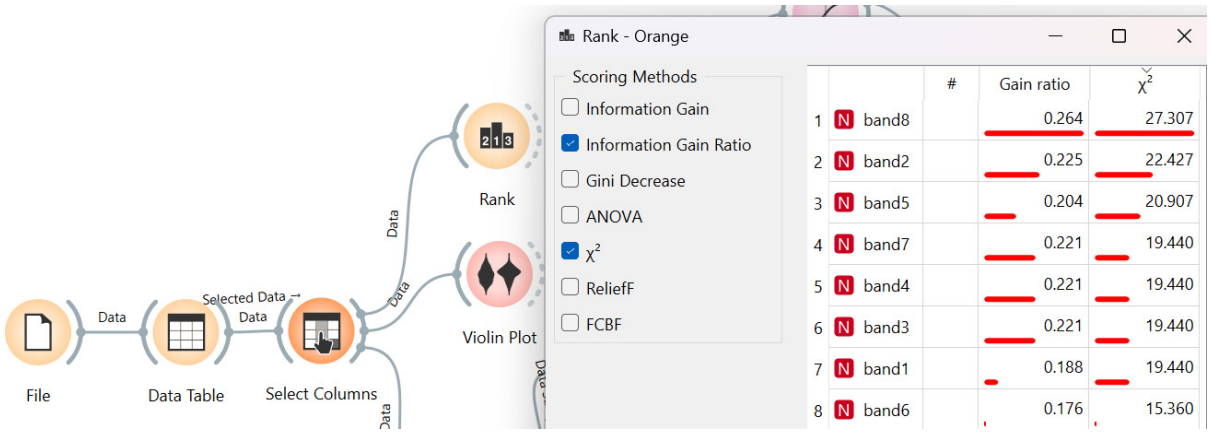

Figure 4. Application of information gain methods

Similarly, it was observed that band 6 provides the least information, with a Gain Ratio value of 0.176 and a percentage contribution of 15.360% in Chi-Square. To further explore the possible relationship between the distribution of reflectance values across the 8 bands of the multispectral image and the categories of the predictor variable (0 or 1), violin plots were utilized via the "Violin Plot" module in Orange (see Figure 5).

doi: 10.25100/iyc.v27i1.14672

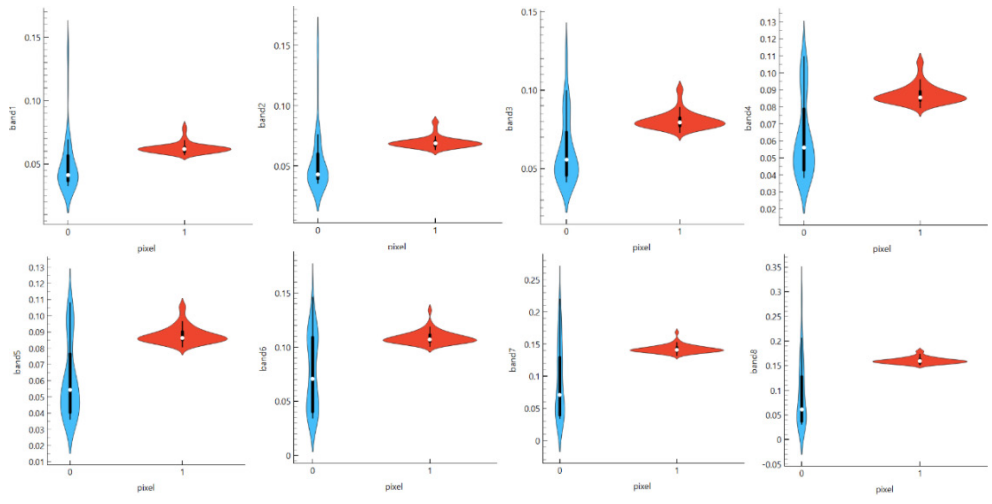

Figure 5. Violin plots of the reflectance bands in the multispectral image

From the violin plots presented in Figure 5, it is evident that the distribution of reflectance values in bands 8, 2, and 5 allows for a clearer differentiation between pixel types 0 (non-asbestos) and 1 (asbestos), as no significant overlap is observed in their densities. This aligns with the results obtained through the Chi-Square method, where these three bands stand out with an information gain percentage exceeding 20.9%.

In comparison, the remaining bands exhibit greater similarity in their distributions, making them less useful for classifying pixel types. Additionally, it is observed that, in general, the reflectance values for pixel type 0 display greater dispersion and variability, whereas those for pixel type 1 exhibit more compact distributions concentrated within narrower ranges. These findings suggest that bands 8, 2, and 5 are particularly effective for distinguishing between asbestos and other materials, consistent with the results obtained using information gain methods.

Once the most relevant reflectance bands were analyzed, the complete workflow for the four machine learning models was deployed using the Orange visual programming tool, as illustrated in Figure 6.

doi: 10.25100/iyc.v27i1.14672

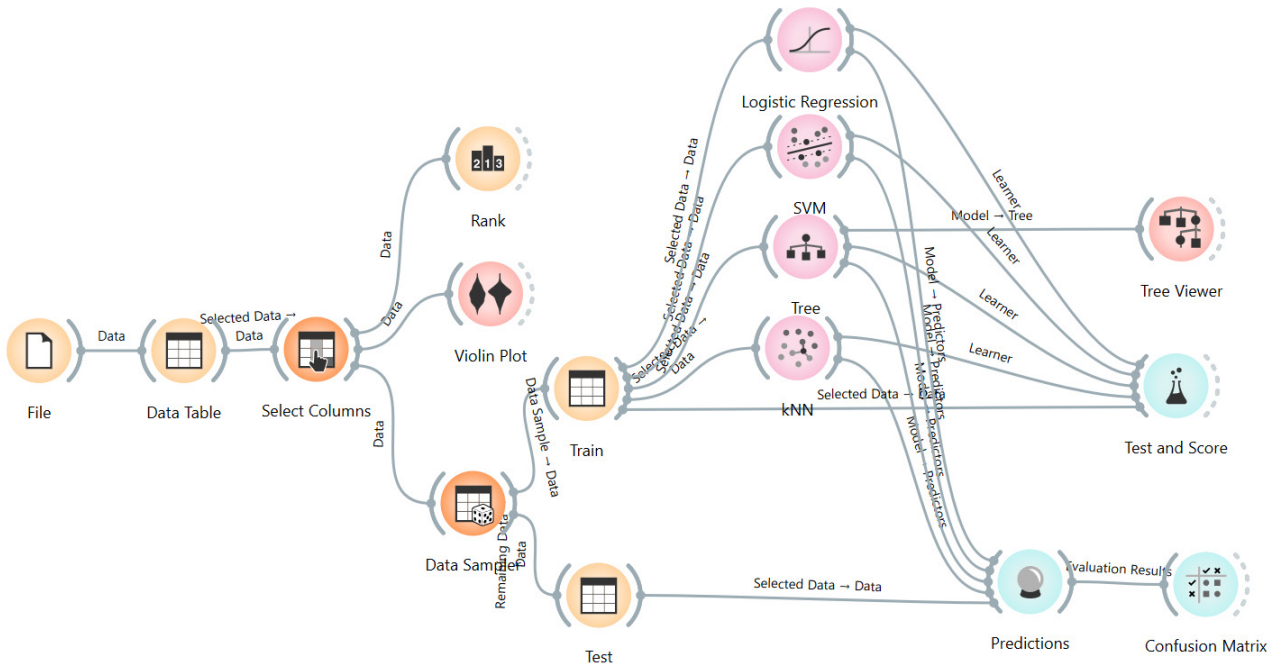

Figure 6. Workflow of machine learning models in Orange

Figure 6 clearly illustrates the various processes carried out in the developed workflow, which include: loading the dataset in Excel format using the "File" module; selecting the 8 attributes (reflectance bands) and the predictor attribute (pixel type) from the dataset's 9 columns using the "Select Columns" module.

Subsequently, information gain methods and violin plots were applied through the "Rank" and "Violin Plot" modules. The dataset was then split into training (70%) and testing (30%) sets using the "Data Sampler" module. The four machine learning models considered (KNN, decision trees, support vector machines, and logistic regression) were trained through the "kNN," "Tree," "SVM," and "Logistic Regression" modules.

Following this, the decision tree diagram was visualized with the "Tree Viewer" module. The models were validated on the training set using the "Test and Score" module and on the testing set using the "Predictions" and "Confusion Matrix" modules. Once the workflow was deployed in the Orange tool, the analysis of the model metrics for the training and testing sets was conducted, as presented in Tables 2 and 3.

Table 2. Results of the models on Train Set Performance

Model	AUC	CA	F1	Precision	Recall
kNN	0.986	0.971	0.971	0.973	0.971
Tree 0.906	0.929	0.928	0.932	0.929	
SVM 1.000	0.943	0.943	0.949	0.943	
Logistic Regression	0.860	0.771	0.759	0.843	0.771

doi: 10.25100/iyc.v27i1.14672

Table 3. Results of the models Test Set Performance

Model	AUC	CA	F1	Precision	Recall
kNN	1.000	1.000	1.000	1.000	1.000
Tree	0.933	0.933	0.933	0.933	0.933
SVM	1.000	1.000	1.000	1.000	1.000
Logistic Regression	0.800	0.833	0.829	0.875	0.833

Considering the results obtained by the models in the Precision and Recall metrics, it is noteworthy that the kNN model with three neighbors, decision trees, and the support vector machine (SVM) model with an RBF kernel achieved the highest values in the training set. Among these, the kNN model showed the best performance, with Precision and Recall metrics of 0.973 and 0.971, respectively, followed by the SVM model with values of 0.949 and 0.943, and the decision tree model with values of 0.932 and 0.939, all demonstrating adequate performance.

In contrast, the logistic regression model achieved Precision and Recall values of 0.843 and 0.771, respectively, indicating more limited performance compared to the other three models. In the testing set, both the kNN and SVM models maintained perfect performance (1.0) in both metrics, while the decision tree model recorded slightly lower values of 0.933 in both Precision and Recall.

This slight decrease in performance for the decision tree model is a positive outcome, as it indicates better generalization capability and a reduced risk of overfitting, emphasizing the importance of achieving more balanced results between the training and testing sets to ensure model robustness. Thus, while all three models with the best performance could be used, the decision tree model demonstrated the highest consistency and was selected for deployment on the entire reference multispectral image. Accordingly, Figure 7 presents the confusion matrix obtained for the selected model.

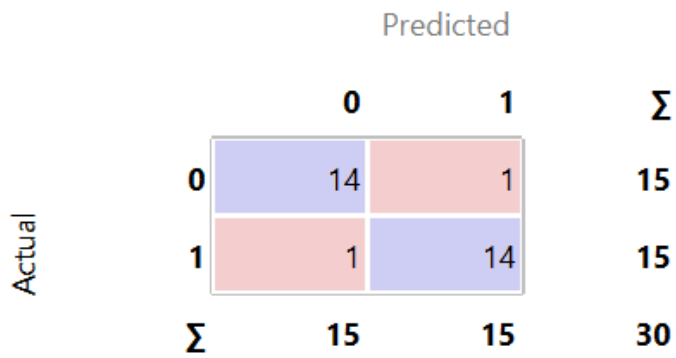

Figure 7. Confusion matrix obtained for the selected decision tree model

Figure 7 shows that, out of a total of 30 instances in the test set (15 asbestos cement and 15 other materials), the decision tree model correctly classified 14 instances as belonging to other materials and misclassified 1 as asbestos cement. For the asbestos cement instances, the model correctly identified 14 of the 15, with one misclassified as belonging to other materials. This corresponds to

doi: 10.25100/iyc.v27i1.14672

a 93.3% accuracy rate in classifying asbestos cement samples, demonstrating adequate performance with a slight error rate in this category.

Additionally, Figure 8 illustrates the decision tree generated by the model, highlighting the attributes identified as most relevant, with bands 8 and 5 being the most significant in the dataset. This aligns with the results obtained through information gain methods and violin plots, where these bands are among the top three most relevant attributes.

Specifically, the rule that enables the classification of asbestos cement pixels (label 1) states that if the reflectance value of band 8 exceeds 0.146159 and that of band 5 is greater than 0.0815123, the model classifies these pixels as belonging to this category, achieving an accuracy of 97.2% (35/36). This result underscores the model's ability to effectively discriminate between classes, particularly in the case of asbestos cement pixels.

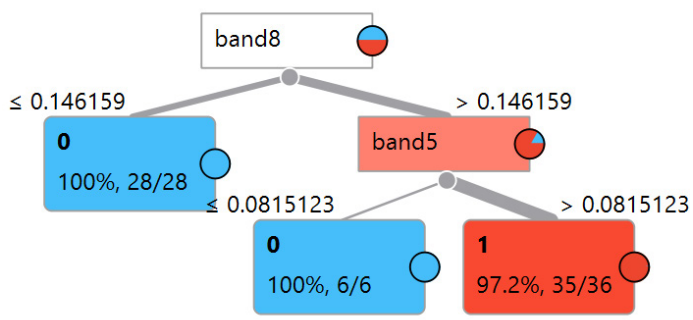

Figure 8. Decision tree obtained by the model

In line with the above, Table 4 presents the three inference rules derived from the decision tree, which relate to bands 8 and 5. These three rules are highly useful for classifying asbestos pixels across the entire image, particularly Rule 3, which pertains to the detection of asbestos cement pixels.

Table 4. Inference rules obtained from the decision tree model

Id	Inference rule
1	If band8 ≤ 0.146159, then the class is 0 (other materials), with 100% accuracy (28/28).
2	If band8 > 0.146159 and band5 ≤ 0.0815123, then the class is 0 (other materials), with 100% accuracy (6/6).
3	If band8 > 0.146159 and band5 > 0.0815123, then the class is 1 (asbestos cement), with 97.2% accuracy (35/36).

Based on the inference rules obtained and presented in Table 4, Rule 3 was applied for the identification of asbestos cement pixels across the total pixels of the reference multispectral image shown in Figure 2, using the Spectral, NumPy, Pandas, and Matplotlib libraries. Figure 9 illustrates the implementation of the asbestos detection method in Python, where the algorithm iterates through each pixel of the image, extracting its 8 spectral bands and applying Inference Rule 3, which involves bands 8 and 5. As a result of this method, Figure 9 highlights in blue the areas detected as containing asbestos cement on the image presented in Figure 2, revealing that 32.4% of the image corresponds to asbestos cement.

doi: 10.25100/iyc.v27i1.14672

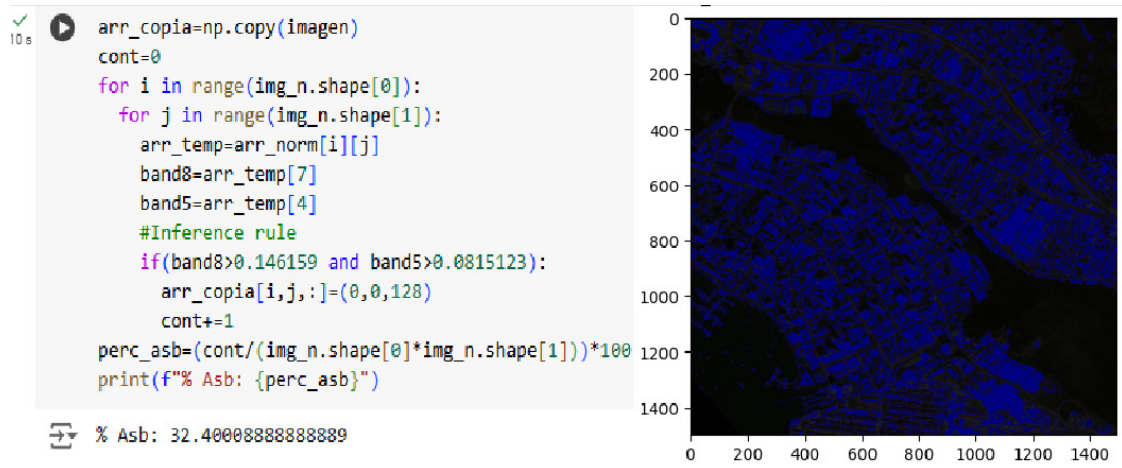

Figure 9. Deployment of the method on the entire image

Discussion

At the level of result discussion and in order to address the first guiding question regarding the performance of the machine learning models evaluated for asbestos-cement detection, it is worth mentioning that this study implemented a machine learning workflow using the Orange tool, employing four models: k-Nearest Neighbors (kNN), decision trees, support vector machines, and logistic regression, for the detection of asbestos-cement in multispectral images. In this regard, it is important to highlight that, on the test set, the kNN, decision tree, and support vector machine models achieved a performance above 0.933 in the Precision, Recall, and F1-Score metrics, whereas the logistic regression model exhibited the lowest performance in these metrics, with values ranging between 0.829 and 0.875. This finding leads to the conclusion that the three best-performing models demonstrate high effectiveness in asbestos-cement detection in multispectral images; however, the decision tree model shows the highest consistency in results across both the training and test sets.

Now, regarding the second guiding question concerning the comparison of the best-performing model with conventional methods in terms of efficacy and efficiency, it is important to highlight that the model that achieved the best balance between performance and consistency across the training and test sets was the decision tree model. This model obtained respective values of 0.932 and 0.929 for Precision and Recall in the training set, while in the test set, it achieved a value of 0.933 for both metrics. Furthermore, this model identified that the relevant bands for asbestos-cement detection are reflectance bands 8 and 5. The identification of these bands is crucial, as it suggests that computational efficiency is optimized through this method by considering only two bands in the inference rule for detection. In contrast, conventional methods, such as the correlation-based approach, use the total number of spectral bands of the image for their calculations, as presented in (47), where similarity is computed between the average or characteristic pixel and the remaining pixels of the image.

Similarly, regarding the third guiding question related to the fields in which the proposed approach can be extrapolated, it is worth mentioning that, since the developed method reduces the

doi: 10.25100/iyc.v27i1.14672

complexity of asbestos-cement identification by using only a pair of bands for detection, it can be applied in research focused on environmental monitoring (14–16), where the area covered by the images is extensive and efficiency is a fundamental requirement.

In this same regard, concerning research focused on asbestos detection using hyperspectral images (48), this study provides a relevant finding, as it demonstrates that with only a few reflectance bands, machine learning methods such as decision trees enable the efficient and effective detection of this material. This not only optimizes computational costs but also reduces expenses in the sample collection process, given that the infrastructure required for capturing and processing hyperspectral images entails a higher economic cost.

Conclusions

Considering that most state-of-the-art research on asbestos cement detection in spectral images has focused on the use of hyperspectral images due to their precision and the extensive spectral information they provide, this article proposes a machine learning-based method for asbestos cement detection within the domain of multispectral satellite images. This method demonstrated not only effective results but also computational efficiency, achieved by utilizing a smaller number of bands and focusing on a reduced set of relevant bands for classifying pixels as asbestos cement. Based on the efficiency achieved by the decision tree model, the proposed approach can be extrapolated to domains where efficiency is paramount, such as environmental monitoring using spectral images, where the images cover large areas, and optimizing processing times is essential.

In this study, four supervised learning models were evaluated: kNN with 3 neighbors, decision trees, support vector machines with an RBF kernel, and logistic regression. The kNN, decision tree, and support vector machine models achieved Precision and Recall metrics above 0.93, with the decision tree model demonstrating the best consistency between the training and testing sets. In addition to its excellent effectiveness in both sets, the decision tree model proved efficient by utilizing an inference rule that involves only band 8 and band 5 for asbestos cement detection, making it competitive with methods such as correlation-based approaches. In this context, the results obtained represent a significant contribution compared to state-of-the-art studies, which predominantly focus on using various methods for asbestos detection in hyperspectral images. The proposed approach enables asbestos detection through an inference rule based on the evaluation of two reflectance bands, which not only optimizes computational costs but also reduces the expenses associated with acquiring and sampling hyperspectral images.

For the development of this research, an adaptation of the CRISP-DM data mining methodology was utilized. To implement the different phases of the methodology, both the Orange visual programming tool and the Python libraries Spectral, NumPy, Pandas, Scikit-learn, and Matplotlib were employed. The mentioned Python libraries were used for constructing the dataset from a reference multispectral image, as well as for deploying the machine learning model on the complete reference image. Meanwhile, the Orange tool was used for applying information gain methods and violin plots, as well as for training and evaluating the four machine learning models considered, following the dataset's division into training and testing sets. The open-source tools

doi: 10.25100/iyc.v27i1.14672

considered for the implementation of the workflow provide a competitive alternative to proprietary software for material detection in spectral images, enabling universities and research centers to replicate and extrapolate these methods in various applications.

As a result of deploying the best-fitting model on the complete reference image corresponding to an area of the city of Cartagena, it was determined that 32.4% of the total pixels in the image were identified as asbestos cement. This result holds significance not only in computational terms but also in the context of public health, given the negative implications of human exposure to fibers from this material. Thus, the findings presented in this article aim to contribute to strategic decision-making regarding asbestos mitigation efforts in Cartagena by government authorities.

On the other hand, it is worth mentioning that, although in the specific case of this study, excellent results were obtained in the detection of asbestos-cement on a multispectral image that was pre-processed by applying the necessary atmospheric corrections, this aspect must be carefully considered, as omitting atmospheric corrections may affect the performance of machine learning models by introducing noise and compromising the discrimination of the spectral signature of asbestos-cement. Similarly, it is important to clarify that pixel sampling is a critical phase of the process, and it is therefore recommended to collect spectral signature samples from areas where visual confirmation is not only assured but where field visits and verification tests have also been conducted to confirm the presence of the material.

As future work, applying the model to other areas of Cartagena and different cities in Colombia and worldwide should be considered. This would allow validating its effectiveness in diverse contexts, strengthening the findings, and expanding the scope of this study. Additionally, evaluating ensemble methods could improve accuracy by leveraging multiple models to enhance predictive capability and robustness.

A comparison of the proposed method's efficiency with non-machine learning approaches is also planned. This would help assess computational cost and processing time, ensuring the model remains practical for large-scale implementations.

CRediT authorship contribution statement

Conceptualization - Ideas: Manuel Saba, Manuel Alejandro Ospina-Alarcón. Data Curation: Gabriel Elías Chanchí-Golondrino. Formal analysis: Gabriel Elías Chanchí-Golondrino. Acquisition of financing: Manuel Saba. Investigation: Manuel Alejandro Ospina-Alarcón, Manuel Saba. Methodology: Manuel Saba, Gabriel Elías Chanchí-Golondrino. Project Management: Manuel Saba. Resources: Manuel Saba. Software: Gabriel Elías Chanchí-Golondrino. Supervision: Manuel Alejandro Ospina-Alarcón. Validation: Manuel Alejandro Ospina-Alarcón. Visualization - Preparation: Gabriel Elías Chanchí-Golondrino. Writing - original draft - Preparation: Gabriel Elías Chanchí-Golondrino, Manuel Alejandro Ospina-Alarcón. Writing - revision and editing - Preparation: Manuel Alejandro Ospina-Alarcón, Manuel Saba.

Conflict of interest: does not declare. Etics Implications: does not declare.

doi: 10.25100/iyc.v27i1.14672

Acknowledgments and funding statement

This article is considered a product within the framework of the project 'DEVELOPMENT OF A COMPREHENSIVE STRATEGY TO REDUCE THE IMPACT ON PUBLIC HEALTH AND THE ENVIRONMENT DUE TO THE PRESENCE OF ASBESTOS IN THE TERRITORY OF THE DEPARTMENT OF BOLÍVAR,' funded by the General Royalties System of Colombia (SGR) and identified with code BPIN 2020000100366. This project was carried out by the University of Cartagena, Colombia, and the Asbestos-Free Colombia Foundation. Finally, the authors would like to express their gratitude to Federico Frassy for his support in the management and classification of hyperspectral data, to Aiken Hernando Ortega Heredia, María Angélica Narváez Cuadro, Carlos Andrés Castrillón Ortiz, Michelle Cecilia Montero Acosta, Margareth Peña Castro, Carlos David Arroyo Angulo, and the rest of the research team for logistical support and sample collection in the field. Additionally, the authors extend their thanks to Juan Manuel González from BlackSquare company for assistance in acquiring hyperspectral data and to Sean Fitzgerald for the PLM analysis

References

1. Guzman-Alvarez JA, González-Zuñiga M, Sandoval Fernandez JA, Calvo-Alvarado JC. Uso de sensores remotos en la agricultura: aplicaciones en el cultivo del banano. Agron Mesoam. 2022 Aug 22;48279. https://doi.org/10.15517/am.v33i3.48279

2. Jiménez-López AF, Jiménez-López M, Jiménez-López FR. Multispectral analysis of vegetation for remote sensing applications. ITECKNE. 2015 Nov;12(2). https://doi.org/10.15332/iteckne.v12i2.1242

3. Awange J, Kiema J. Fundamentals of Remote Sensing. In 2019. p. 115-23. https://doi.org/10.1007/978-3-030-03017-9_7

4. Fang Q, Han D, Wang Z. Cross-Modality Fusion Transformer for Multispectral Object Detection. SSRN Electron J. 2022; https://doi.org/10.2139/ssrn.4227745

5. Zhang H, Fromont E, Lefevre S, Avignon B. Multispectral Fusion for Object Detection with Cyclic Fuse-and-Refine Blocks. In: 2020 IEEE International Conference on Image Processing (ICIP). IEEE; 2020. p. 276-80. https://doi.org/10.1109/ICIP40778.2020.9191080

6. Hu S, Bonardi F, Bouchafa S, Prendinger H, Sidibé D. Rethinking Self-Attention for Multispectral Object Detection. IEEE Trans Intell Transp Syst. 2024 Nov;25(11):16300-11. https://doi.org/10.1109/TITS.2024.3412417

7. Takumi K, Watanabe K, Ha Q, Tejero-De-Pablos A, Ushiku Y, Harada T. Multispectral Object Detection for Autonomous Vehicles. In: Proceedings of the on Thematic Workshops of ACM Multimedia 2017. New York, NY, USA: ACM; 2017. p. 35-43. https://doi.org/10.1145/3126686.3126727

8. Sánchez-Méndez AG, Arguijo-Hernández SP. Análisis de imágenes multiespectrales para la detección de cultivos y detección de plagas y enfermedades en la producción de café. Res Comput Sci. 2018 Dec;147(7):309-17. https://doi.org/10.13053/rcs-147-7-24

9. Pelaez Carrillo DA, Gualdron Guerrero OE, Torres Chavez I. Optimización de la evaluación de pastos mediante la implementación de imágenes multiespectrales y vehículo aéreo no tripulado.

Rev Colomb Tecnol Av. 2024 May;1(43):155-62. https://doi.org/10.24054/rcta.v1i43.2850

10. Meneses VAB, Téllez JM, Velasquez DFA. Uso de drones para el análisis de imágenes multiespectrales en agricultura de precisión. limentech, Cienc y Tecnol Aliment. 2017 Sep;13(1). https://doi.org/10.24054/01204211.v1.n1.2015.1647

11. Eugenio FC, Grohs M, Schuh MS, Venancio LP, Schons C, Badin TL, et al. Flooded rice variables from high-resolution multispectral images and machine learning algorithms. Remote Sens Appl Soc Environ. 2023 Aug;31:100998. https://doi.org/10.1016/j.rsase.2023.100998

12. Ormazábal Y, Ávila C, Mena C, Morales Y, Bustos Ó. Caracterización y cuantificación de fragmentos de bosque nativo, en un sector del secano interior de la Región del Maule, Chile. Ciência Florest. 2013 Aug;23(3):449-60. https://doi.org/10.5902/1980509810556

13. Ngo DT. Mapping tree species of wetlands using multispectral images of UAVs and machine learning: A case study of the Dong Rui Commune. Heliyon. 2024 Aug;10(15):e35159. https://doi.org/10.1016/j.heliyon.2024.e35159

14. Peña MA. Propiedades del primer sistema de teledetección hiperespectral chileno. Rev Geogr Norte Gd. 2010 Sep;(46). https://doi.org/10.4067/S0718-34022010000200011

15. Lu B, He Y, Dao PD. Comparing the Performance of Multispectral and Hyperspectral Images for Estimating Vegetation Properties. IEEE J Sel Top Appl Earth Obs Remote Sens. 2019 Jun;12(6):1784-97. https://doi.org/10.1109/JSTARS.2019.2910558

16. He J, Yuan Q, Li J, Zhang L. A Knowledge Optimization-Driven Network With Normalizer-Free Group ResNet Prior for Remote Sensing Image Pan-Sharpening. IEEE Trans Geosci Remote Sens. 2022;60:1-16. https://doi.org/10.1109/TGRS.2022.3230846

17. Chaparro JE, Aedo JE, Lumbreras Ruiz F. Machine Learning for the estimation of foliar nitrogen content in pineapple crops using multispectral images and Internet of Things (IoT) platforms. J Agric Food Res. 2024 Dec;18:101208. https://doi.org/10.1016/j.jafr.2024.101208

18. Pinheiro Claro Gomes W, Gonçalves L, Barboza da Silva C, Melchert WR. Application of multispectral imaging combined with machine learning models to discriminate special and traditional green coffee. Comput Electron Agric. 2022 Jul;198:107097.

https://doi.org/10.1016/j.compag.2022.107097

19. Schulte to Bühne H, Pettorelli N. Better together: Integrating and fusing multispectral and radar satellite imagery to inform biodiversity monitoring, ecological research and conservation science. Lecomte N, editor. Methods Ecol Evol. 2018 Apr;9(4):849-65.

https://doi.org/10.1111/2041-210X.12942

20. Galán-Cuenca Á, Vázquez-Martín R, Mandow A, Morales J, García-Cerezo A. Análisis de técnicas de aumento de datos y entrenamiento en YOLOv3 para detección de objetos en imágenes RGB y TIR del UMA-SAR Dataset. In: XLII Jornadas De Automática: Libro De Actas. Servizo de Publicacións da UDC; 2021. p. 686-94.

https://doi.org/10.17979/spudc.9788497498043.686

21. van der Meer FD, van der Werff HMA, van Ruitenbeek FJA, Hecker CA, Bakker WH, Noomen MF, et al. Multi- and hyperspectral geologic remote sensing: A review. Int J Appl Earth Obs Geoinf. 2012 Feb;14(1):112-28. https://doi.org/10.1016/j.jag.2011.08.002

22. Peyghambari S, Zhang Y. Hyperspectral remote sensing in lithological mapping, mineral exploration, and environmental geology: an updated review. J Appl Remote Sens. 2021 Jul 14;15(03). https://doi.org/10.1117/1.JRS.15.031501

23. Sabat M, Fares N, Mitri G, Kfoury A. Determination of asbestos cement rooftop surface composition using regression analysis and hyper-spectral reflectance data in the visible and near-infrared ranges. J Hazard Mater. 2024 May;469:134006.

https://doi.org/10.1016/j.jhazmat.2024.134006

24. Bassani C, Cavalli RM, Cavalcante F, Cuomo V, Palombo A, Pascucci S, et al. Deterioration status of asbestos-cement roofing sheets assessed by analyzing hyperspectral data. Remote Sens Environ. 2007 Aug;109(3):361-78.

https://doi.org/10.1016/j.rse.2007.01.014

25. Cilia C, Panigada C, Rossini M, Candiani G, Pepe M, Colombo R. Mapping of Asbestos Cement Roofs and Their Weathering Status Using Hyperspectral Aerial Images. ISPRS Int J Geo-Information. 2015 Jun 1;4(2):928-41.

https://doi.org/10.3390/ijgi4020928

26. Kaplan G, Gašparović M, Kaplan O, Adjiski V, Comert R, Mobariz MA. Machine Learning-Based Classification of Asbestos-Containing Roofs Using Airborne RGB and Thermal Imagery. Sustainability. 2023 Mar;15(7):6067. https://doi.org/10.3390/su15076067

27. Magnani C, Mensi C, Binazzi A, Marsili D, Grosso F, Ramos-Bonilla JP, et al. The Italian Experience in the Development of Mesothelioma Registries: A Pathway for Other Countries to Address the Negative Legacy of Asbestos. Int J Environ Res Public Health. 2023 Jan;20(2):936. https://doi.org/10.3390/ijerph20020936

28. Mensi C, Riboldi L, De Matteis S, Bertazzi PA, Consonni D. Impact of an asbestos cement factory on mesothelioma incidence: Global assessment of effects of occupational, familial, and environmental exposure. Environ Int. 2015 Jan;74:191-9.

https://doi.org/10.1016/j.envint.2014.10.016

29. Luberto F, Ferrante D, Silvestri S, Angelini A, Cuccaro F, Nannavecchia AM, et al. Cumulative asbestos exposure and mortality from asbestos related diseases in a pooled analysis of 21 asbestos cement cohorts in Italy. Environ Heal. 2019 Dec;18(1):71.

https://doi.org/10.1186/s12940-019-0510-6

30. Martel E, Guerra R, Lopez S, Sarmiento R. A GPU-Based Processing Chain for Linearly Unmixing Hyperspectral Images. IEEE J Sel Top Appl Earth Obs Remote Sens. 2017 Mar;10(3):818-34.

https://doi.org/10.1109/JSTARS.2016.2614842

31. Toma AC, Panica S, Zaharie D, Petcu D. Computational challenges in processing large hyperspectral images. In: 2012 5th Romania Tier 2 Federation Grid, Cloud & High Performance Computing Science (RQLCG). 2012. p. 111-4.

32. Paoletti ME, Haut JM, Plaza J, Plaza A. Estudio Comparativo de Técnicas de Clasificación de Imágenes Hiperespectrales. Rev Iberoam Automática e Informática Ind. 2019 Mar;16(2):129.

https://doi.org/10.4995/riai.2019.11078

33. Mohan BK, Porwal A. Hyperspectral Image Processing and Analysis. Curr Sci. 2015;108(5):833-41. https://www.citedi.mx/percepcionremota/portal/files/documents/HA17082404.pdf

34. Ibarrola-Ulzurrun E, Marcello-Ruiz FJ, Gonzalo-Martín C. Evaluation of dimensionality reduction techniques in hyperspectral imagery and their application for the classification of terrestrial

doi: 10.25100/iyc.v27i1.14672

ecosystems. In: Bruzzone L, Bovolo F, Benediktsson JA, editors. Image and Signal Processing for Remote Sensing XXIII. SPIE; 2017. p. 17. https://doi.org/10.1117/12.2278501

35. Race BR, Wittman T. A comparison of dimensionality reduction techniques for hyperspectral imagery. In: Messinger DW, Velez-Reyes M, editors. Algorithms, Technologies, and Applications for Multispectral and Hyperspectral Imaging XXVIII. SPIE; 2022. p. 53.

https://doi.org/10.1117/12.2632014

36. Bravo Martínez G, Silva Aceves JM, Torres Argüelles SV, Enríquez Aguilera FJ. Implementación de Algoritmos de Procesamiento Digital de Señales en Hardware Paralelo: Artículo de revisión. Cult Científica y Tecnológica. 2018;(66):80-100.

https://doi.org/10.20983/culcyt.2018.3.10

37. Altamimi A, Ben Youssef B. A Systematic Review of Hardware-Accelerated Compression of Remotely Sensed Hyperspectral Images. Sensors. 2021 Dec 30;22(1):263.

https://doi.org/10.3390/s22010263

38. Nalepa J. Recent Advances in Multi- and Hyperspectral Image Analysis. Sensors. 2021 Sep 8;21(18):6002. https://doi.org/10.3390/s21186002

39. Viel F, Parreira WD, Susin AA, Zeferino CA. A Hardware Accelerator for Onboard Spatial Resolution Enhancement of Hyperspectral Images. IEEE Geosci Remote Sens Lett. 2021 Oct;18(10):1796-800. https://doi.org/10.1109/LGRS.2020.3009019

40. Reena Thakur E al. A Comprehensive Analysis to Image Classification: Understanding Techniques and Explore Data Preprocessing a Non-linear Approach. Adv Nonlinear Var Inequalities. 2023 Jun;26(2):110-22. https://doi.org/10.52783/anvi.v26.i2.287

41. Martinez-Plumed F, Contreras-Ochando L, Ferri C, Hernandez-Orallo J, Kull M, Lachiche N, et al. CRISP-DM Twenty Years Later: From Data Mining Processes to Data Science Trajectories. IEEE Trans Knowl Data Eng. 2021 Aug 1;33(8):3048-61.

https://doi.org/10.1109/TKDE.2019.2962680

42. Schröer C, Kruse F, Gómez JM. A Systematic Literature Review on Applying CRISP-DM Process Model. Procedia Comput Sci. 2021;181:526-34. https://doi.org/10.1016/j.procs.2021.01.199

43. Maataoui S, Bencheikh G, Bencheikh G. Predictive Maintenance in the Industrial Sector: A CRISP-DM Approach for Developing Accurate Machine Failure Prediction Models. In: 2023 Fifth International Conference on Advances in Computational Tools for Engineering Applications (ACTEA). IEEE; 2023. p. 223-7. https://doi.org/10.1109/ACTEA58025.2023.10193983

44. Nava J, Hernández P. Optimization of a Hybrid Methodology (CRISP-DM). In: Logistics Management and Optimization through Hybrid Artificial Intelligence Systems. IGI Global; 2012. p. 356-79. https://doi.org/10.4018/978-1-4666-0297-7.ch014

45. Lin C-H, Hsieh C-Y, Lin J-T. CODE-IF: A Convex/Deep Image Fusion Algorithm for Efficient Hyperspectral Super-Resolution. IEEE Trans Geosci Remote Sens. 2024;62:1-18.

https://doi.org/10.1109/TGRS.2024.3384808

46. Halimu C, Kasem A, Newaz SHS. Empirical Comparison of Area under ROC curve (AUC) and Mathew Correlation Coefficient (MCC) for Evaluating Machine Learning Algorithms on Imbalanced Datasets for Binary Classification. In: Proceedings of the 3rd International Conference on Machine Learning and Soft Computing. New York, NY, USA: ACM; 2019. p. 1-6.

https://doi.org/10.1145/3310986.3311023

doi: 10.25100/iyc.v27i1.14672

47. Chanchí Golondrino GE, Ospina Alarcón MA, Saba M. Vegetation Identification in Hyperspectral Images Using Distance/Correlation Metrics. Atmosphere (Basel). 2023 Jul 14;14(7):1148.

https://doi.org/10.3390/atmos14071148

48. Saba M, Valdelamar Martínez D, Torres Gil LK, Chanchí Golondrino GE, Alarcón MAO. Application of Supervised Learning Methods and Information Gain Methods in the Determination of Asbestos-Cement Roofs' Deterioration State. Appl Sci. 2024 Sep 19;14(18):8441.

https://doi.org/10.3390/app14188441

doi: 10.25100/iyc.v27i1.14672